

ELASTOSTATIC BENDING OF A 2D-FGSW BEAM UNDER NONUNIFORM DISTRIBUTED LOADS

Nguyen Van Chinh^{1,*}, Le Cong Ich¹, Le Thi Ngoc Anh^{2,3}, Nguyen Dinh Kien^{3,4}

¹Le Quy Don Technical University, 236 Hoang Quoc Viet, Ha Noi

²Institute of Applied Information and Mechanics, 291 Dien Bien Phu, Ho Chi Minh City

³Graduate University of Science and Technology, VAST, 18 Hoang Quoc Viet, Ha Noi

⁴Institute of Mechanics, VAST, 18 Hoang Quoc Viet, Ha Noi

*Email: ngchinhhd@gmail.com

Received: 31 December 2018; Accepted for publication: 18 April 2019

Abstract. Elastostatic bending behavior of a two-directional functionally graded sandwich (2D-FGSW) beam under various types of nonuniform distributed load is studied. The beam is considered to be formed from a pure ceramic hardcore and two-directional functionally graded (2D-FG) skin layers. Based on a 3D-quasi shear deformation theory, a finite element model is derived and employed in the study. Elastostatic response of the beam is computed for the beam with different boundary conditions and aspect ratio. The effects of the material distribution and the loading type on the deflections and stresses distribution are investigated and highlighted. The influence of the aspect ratio on the behavior of the beam is also examined and discussed.

Keywords: 2D-FGSW beam, 3D-quasi theory, elastostatic bending, nonuniform distributed load, finite element model.

Classification numbers: 2.9.4, 5.4.2, 5.4.3.

1. INTRODUCTION

Functionally graded materials (FGMs), a new type of advanced composites initiated by Japanese researchers in mid-1980, are increasingly used as structural components in aerospace, energy and automotive reactor industries. FGMs are formed by continuously and smoothly varying constituent materials, usually ceramics and metals, in one or more desired spatial directions. The physical and mechanical properties of the resulted materials are continuous functions of the spatial coordinates, and this feature enables the materials to overcome the drawbacks such as delaminating and stress concentration which are often seen in conventional laminated fiber reinforced composites.

Beam as a major part in many structures are often subjected to various types of external loads. In order to improve the performance of beam, FGMs are widely employed to fabricate this kind of structural component for use in severe environment. Comprehending the mechanical

behavior of FGM beams under different types of loading is crucial for efficient design of structures. Many investigations on free vibration [1-5], forced vibration [6-10], bending [11-15], buckling [16-18] behavior of FGM beam have been reported in recent years. The material properties of the beams in the above cited references are considered to vary in only one direction, the thickness or the longitudinal direction of the beams.

In many practical circumstances where the conventional one-directional FGMs (1D-FGMs) are not sufficient for optimizing the structures [19]. For example, the temperature and stress distribution of an aerospace craft vary in both the thickness and length of the craft. The development of FGMs with material properties varying in two or three directions is, thus of great importance in practice. Investigation on vibration and bending behavior of two-directional functionally graded (2D-FGM) beams has been extensively carried out in recent years. Lü *et al.* [20] studied bending of a 2D-FGM beam by considering its Young's modulus varying in the thickness and length directions by an exponential law. A semi-analytical elasticity solution was derived by the authors to show the effects of material distribution on the deflection and axial stress of the beam. Also assuming an exponential-law variation for the material properties in the beam length and thickness, Simşek [21] studied dynamic behavior of a 2D-FGM beam due to a moving load. The numerical result obtained by the author reveals that the 2D-FGM beam can be tailored to meet the design goals of optimizing the dynamic response. The dynamic stiffness method was employed by Hao and Wei [22] to study free and forced vibration of 2D-FGM Timoshenko beams with the material properties being graded in axial and thickness direction by an exponential law. The natural frequencies and dynamic response of the beams under a moving harmonic load were obtained in the work by the Wittrick-William algorithm and modal superposition method, respectively. Lezgy-Nazargah [23] employed the NURBS isogeometric finite element method to examine the thermal stress in exponential 2D-FGM beams subjected to different types of non-uniform temperature field. The free vibration of a power-law 2D-FGM beam was investigated by Wang *et al.* [24] by an analytical method. The authors showed that a critical frequency, which depends on the material indexes, is existed and the natural frequencies have an abrupt jump when across the critical frequency. Nguyen *et al.* [25] studied the dynamic response of 2D-FGM Timoshenko beams by a finite element method. The finite element method was also employed in [26, 27] to study free vibration of 2D-FDG beams. Displacements and stresses of 2D-FGM circular beams due to static bending were obtained by Pydah and Sabale [28] using an analytical method. The static bending of 2D-FGM beams with exponential variation of Young's modulus was also studied in [29] by using the smooth particle hydrodynamics method. The generalized differential quadrature method was employed by Tang *et al.* [30] to predict vibration modes and nonlinear frequencies of power-law 2D-FGM beams.

Sandwich structures with the advantage of high strength-to-weight ratio are widely employed in aerospace application such as skin of wings, aileron, and spoilers. To improve the performance of these structures in thermal environment, FGMs can be incorporated in the sandwich fabrication. Investigations on mechanical behavior of functionally graded sandwich (FGSW) beams have been carried out by several authors in recent years. In this line of works, Bui *et al.* [31] employed the mesh free radial point interpolation method to study dynamic response of sandwich beam with a power-law FGM core. The authors employed Mori-Tanaka scheme to evaluate the effective material properties and the penalty technique to treat the discontinuities between the layers. Based on Reddy-Birkford shear deformation theory, Vo *et al.* [32] presented a finite element model for studying free vibration and buckling of FGSW beams. Natural frequencies and buckling loads were evaluated for the beams formed from a homogeneous core and two power-law functionally graded skin layers. In [33, 34], the vibration and static bending of FGSW beams were studied by a quasi-3D shear deformation theory, a

theory extended from the Reddy-Birkford theory by including the thickness stretching effect. Based on a co-rotational finite element formulation, Nguyen and Tran [35] investigated bending behavior of FGSW beams and frames undergoing the large deformations. Free vibration of the first-order shear deformable FGSW beams resting on Pasternak foundation was considered by Su [36] by a modified Fourier series method. Both Voigt model and Mori-Tanaka scheme have been employed by the author to evaluate the effective material properties of the beams. Recently, Karamanli [37] adopted the quasi-3D theory to derive the equilibrium equations for bending of a two-directional functionally graded sandwich (2D-FGSW) beam under uniform distributed loads. The response of the beam has been computed with the aid of the symmetric smoothed particle hydrodynamics method to compute the deflections and stresses.

The above literature review shows that there is only one study on behavior of the 2D-FGSW beams carried out by Karamanli in [37] by using the symmetric smoothed particle hydrodynamics method so far. In this paper, the elastostatic bending behavior of a 2D-FGSW beam under various types on nonuniform distributed loads is further considered by the finite element method. The beams considered in the present work is assumed to be formed from a homogeneous ceramic hardcore and 2D-FG skin layers. The material properties of the skin layers are assumed to vary in both the thickness and longitudinal directions by a power law. Based on the quasi-3D shear deformation theory, a two-node finite element formulation with six degrees of freedom per node is derived and employed to compute the deflections and stresses of the beam. It is necessary to mention that, in addition to the nonuniform distributed loads considered herein, the finite element method used in the present paper are the two main features which are different from that of Ref. [37]. Numerical results in terms of deflections and stresses are given in tabular and graphics, and the effects of material distribution, the loading type as well as the skin-core-skin thickness ratio on the behavior of the beams are investigated and discussed.

2. 2D-FGSW BEAM

Figure 1 shows a 2D-FGSW beam with length L , rectangular cross section ($b \times h$) in a Cartesian coordinate (x, z), where x -axis is chosen in the mid-plane. The beam is assumed to be formed from a homogeneous ceramic hardcore and two 2D-FG skin layers. Denoting z_0, z_1, z_2 and z_3 are, respectively, the coordinates of the bottom surface, layer interfaces and top surface, in with $z_0 = -h/2$ and $z_3 = h/2$.

The FGM of the two skin layers is assumed to be formed from ceramic and metal whose volume fraction varies in both the thickness and longitudinal directions according to [37].

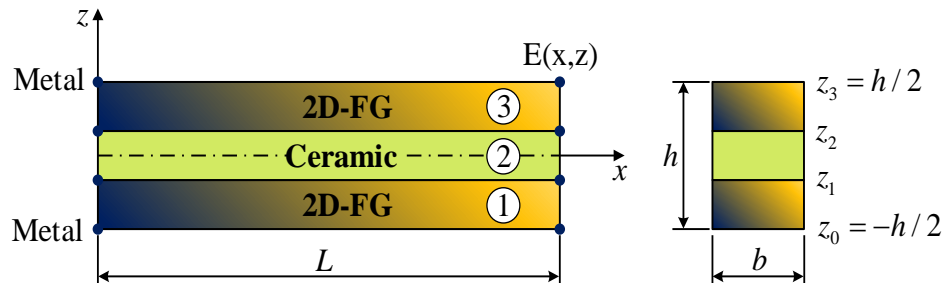


Figure 1. A 2D-FGSW in a Cartesian coordinate system.

$$V_m = \begin{cases} \left(\frac{z-z_1}{z_0-z_1} \right)^{p_z} \left(1 - \frac{x}{2L} \right)^{p_x} & \text{for } z \in [z_0, z_1] \\ 0 & \text{for } z \in [z_1, z_2] \\ \left(\frac{z-z_2}{z_3-z_2} \right)^{p_z} \left(1 - \frac{x}{2L} \right)^{p_x} & \text{for } z \in [z_2, z_3] \end{cases} \quad (1)$$

and
$$V_c(x, z) = 1 - V_m(x, z) \quad (2)$$

In the above equations, V_m and V_c are, respectively, the volume fraction of the metal and ceramic; p_x and p_z are the material grading indexes, defining the variation of the constituents in the x - and z -direction, respectively. Noting that when $p_x = 0$ the beam deduces to the conventional 1D-FGSW beam with the material properties vary in the thickness direction only.

The effective property, $P(x, z)$, evaluated by Voigt model is of the forms

$$P(x, z) = \begin{cases} (P_m - P_c) \left(\frac{z-z_1}{z_0-z_1} \right)^{p_z} \left(1 - \frac{x}{2L} \right)^{p_x} + P_c & \text{if } z \in [z_0, z_1] \\ P_c & \text{if } z \in [z_1, z_2] \\ (P_m - P_c) \left(\frac{z-z_2}{z_3-z_2} \right)^{p_z} \left(1 - \frac{x}{2L} \right)^{p_x} + P_c & \text{if } z \in [z_2, z_3] \end{cases} \quad (3)$$

where P_m and P_c are the properties of the metal and ceramic, respectively.

3. MATHEMATICAL MODELS

Based on the quasi-3D shear deformation theory which includes both shear deformation and thickness stretching effects, the displacements in the x - and z -directions, $u_1(x, z)$ and $u_3(x, z)$, respectively are given by [33, 34]

$$\begin{aligned} u_1(x, z) &= u(x) - zw_{b,x}(x) - f(z)w_{s,x}(x) \\ u_3(x, z) &= w_b(x) + w_s(x) + g(z)w_z(x) \end{aligned} \quad (4)$$

where u_0 , w_b , w_s and w_z are unknown displacements of a point on the mid-plane, and

$$f(z) = \frac{4z^3}{3h^2}, \quad g(z) = 1 - \frac{4z^2}{h^2} \quad (5)$$

In Eq. (4) and hereafter, a subscript comma is used to denote the derivative with respect to the followed variable, e.g. $w_{b,x} = \partial w_b / \partial x$, $w_{s,xx} = \partial^2 w_s / \partial x^2$. Noting that if $g(z)=0$ the displacement field given by Eq. (4) returns to the displacements of Reddy-Bickford theory [38, 39].

The strain components resulted from Eq. (4) gives are of the forms

$$\begin{aligned} \varepsilon_x &= u_{1,x} = u_{,x} - zw_{b,xx} - \frac{4z^3}{3h^2}w_{s,xx}, \quad \varepsilon_z = u_{3,z} = -\frac{8z}{h^2}w_z \\ \gamma_{xz} &= u_{1,z} + u_{3,x} = \left(1 - \frac{4z^2}{h^2} \right) (w_{s,x} + w_{z,x}) \end{aligned} \quad (6)$$

Based on Hook's law, the constitutive equations are given by

$$\begin{Bmatrix} \sigma_x \\ \sigma_z \\ \tau_{xz} \end{Bmatrix} = \begin{bmatrix} Q_{11} & Q_{13} & 0 \\ Q_{13} & Q_{11} & 0 \\ 0 & 0 & Q_{55} \end{bmatrix} \begin{Bmatrix} \varepsilon_x \\ \varepsilon_z \\ \gamma_{xz} \end{Bmatrix} \quad (7)$$

with

$$Q_{11} = \frac{E(x, z)}{1 - \nu^2}, \quad Q_{13} = \frac{\nu E(x, z)}{1 - \nu^2}, \quad Q_{55} = \frac{E(x, z)}{2(1 + \nu)} \quad (8)$$

where ν is the Poisson's ratio, which assumed to be constant.

The strain energy of the beam is given by

$$U = \frac{1}{2} \int_V (\sigma_x \varepsilon_x + \sigma_z \varepsilon_z + \tau_{xz} \gamma_{xz}) dV \quad (9)$$

with V is the volume of the beam. Substituting Eqs. (6) and (7) into Eq. (9), one gets the expression for the strain energy of the beam in the form

$$\begin{aligned} U = & \frac{1}{2} \int_0^L \left[A_{11} u_{,x}^2 - 2A_{12} u_{,x} w_{b,xx} + A_{22} \left(w_{b,xx}^2 + \frac{64}{h^4} w_z^2 \right) - \frac{8}{3h^2} A_{23} u_{,x} w_{s,xx} + \frac{8}{3h^2} A_{44} w_{b,xx} w_{s,xx} \right. \\ & \left. + \frac{16}{9h^4} A_{66} w_{s,xx}^2 + \frac{16}{h^2} \left(-B_{12} u_{,x} w_z + B_{22} w_{b,xx} w_z + \frac{4}{3h^2} B_{44} w_{s,xx} w_z \right) \right. \\ & \left. + \left(C_{11} - \frac{8}{h^2} C_{22} + \frac{16}{h^4} C_{44} \right) (w_{b,x} + w_{s,x})^2 \right] dx \end{aligned} \quad (10)$$

In the above equation, $A_{11}, A_{12}, \dots, C_{22}, C_{44}$ are the beam rigidities, which are defined as

$$(A_{11}, A_{12}, A_{22}, A_{23}, A_{44}, A_{66}) = b \sum_{i=1}^3 \int_{z_{i-1}}^{z_i} Q_{11}(1, z, z^2, z^3, z^4, z^6) dz \quad (11)$$

$$(B_{12}, B_{22}, B_{44}) = b \sum_{i=1}^3 \int_{z_{i-1}}^{z_i} Q_{13}(z, z^2, z^4) dz \quad (12)$$

and

$$(C_{11}, C_{22}, C_{44}) = b \sum_{i=1}^3 \int_{z_{i-1}}^{z_i} Q_{55}(z, z^2, z^4) dz \quad (13)$$

with A is the cross-sectional area.

The work done by the distributed load $q(x)$ has a simple form

$$V = \int_0^L w q(x) dx = \int_0^L (w_b + w_s + w_z) q(x) dx \quad (14)$$

A system of equilibrium equations can be obtained by applying the potential energy principle to Eqs. (10) and (14). However, due to the rigidities $A_{11}, A_{12}, \dots, C_{22}, C_{44}$ as defined by Eqs. (11)-(13) are function of x , and a closed-form solution for such equations is very difficult to be obtained. A finite element model is developed herein to compute the response of the beam.

4. FINITE ELEMENT FORMULATION

A two-node beam element with length of ℓ is derived in this section for computing the response of the 2D-FGSW beam. The element contains six degrees of freedom per node, and the vector of nodal displacements has twelve components as

$$\mathbf{d} = \{u_1 \ w_{b1} \ w_{s1} \ w_{z1} \ \theta_{b1} \ \theta_{s1} \ u_2 \ w_{b2} \ w_{s2} \ w_{z2} \ \theta_{b2} \ \theta_{s2}\}^T \quad (15)$$

where, in addition to the axial and transverse displacements, the rotations stemming from the bending and shear deflections are introduced as

$$\theta_b = w_{b,x}, \quad \theta_s = w_{s,x} \quad (16)$$

In Eq. (15) and hereafter, a superscript ' T ' is used to indicate the transpose of a vector or a matrix. The displacements and rotations inside the element are interpolated from the nodal values according to

$$\{u \ w_b \ w_s \ w_z \ \theta_b \ \theta_s\}^T = \mathbf{N}^T \mathbf{d} \quad (17)$$

where \mathbf{N} is the matrix of interpolation functions with the following form. In the present work, linear functions are employed for the displacements u and w_z , while cubic Hermite polynomials are used for w_b and w_s . In this regard, the matrix \mathbf{N} can be written as

$$\mathbf{N} = \begin{bmatrix} N_1 & 0 & 0 & 0 & 0 & 0 & N_4 & 0 & 0 & 0 & 0 & 0 \\ 0 & N_2 & 0 & 0 & N_3 & 0 & 0 & N_5 & 0 & 0 & N_6 & 0 \\ 0 & 0 & N_2 & 0 & 0 & N_3 & 0 & 0 & N_5 & 0 & 0 & N_6 \\ 0 & 0 & 0 & N_1 & 0 & 0 & 0 & 0 & 0 & N_4 & 0 & 0 \\ 0 & N_{2,x} & 0 & 0 & N_{3,x} & 0 & 0 & N_{5,x} & 0 & 0 & N_{6,x} & 0 \\ 0 & 0 & N_{2,x} & 0 & 0 & N_{3,x} & 0 & 0 & N_{5,x} & 0 & 0 & N_{6,x} \end{bmatrix} \quad (18)$$

with

$$\begin{aligned} N_1 &= 1 - \frac{x}{\ell}, & N_2 &= 1 - 3\frac{x^2}{\ell^2} + 2\frac{x^3}{\ell^3}, & N_3 &= x - 2\frac{x^2}{\ell} + \frac{x^3}{\ell^2} \\ N_4 &= \frac{x}{\ell}, & N_5 &= 3\frac{x^2}{\ell^2} - 2\frac{x^3}{\ell^3}, & N_6 &= -\frac{x^2}{\ell} + \frac{x^3}{\ell^2} \end{aligned} \quad (19)$$

The use of the above cubic Hermite polynomials to interpolate the transverse displacement prevents the element from the shear locking. Using the interpolation scheme (17)-(19), one can write the strain energy of the beam given by Eq. (10) in the form

$$U = \frac{1}{2} \sum^{\text{nELE}} \mathbf{d}^T \mathbf{k} \mathbf{d} \quad (20)$$

where 'nELE' is the total number of the elements used to discrete the beam, and \mathbf{k} is the element stiffness matrix with the following form

$$\begin{aligned}
 \mathbf{k} = & \int_0^\ell \left[A_{11} (\mathbf{N}_{,x}^{(1)})^T \mathbf{N}_{,x}^{(1)} - A_{12} (\mathbf{N}_{,x}^{(1)})^T \mathbf{N}_{,xx}^{(2)} + A_{22} \left((\mathbf{N}_{,xx}^{(2)})^T \mathbf{N}_{,xx}^{(2)} + \frac{64}{h^4} (\mathbf{N}^{(4)})^T \mathbf{N}^{(4)} \right) \right. \\
 & - \frac{8}{3h^2} A_{23} (\mathbf{N}_{,x}^{(1)})^T \mathbf{N}_{,xx}^{(3)} - \frac{8}{3h^2} A_{44} (\mathbf{N}_{,xx}^{(2)})^T \mathbf{N}_{,xx}^{(3)} + \frac{16}{9h^4} A_{66} (\mathbf{N}_{,xx}^{(3)})^T \mathbf{N}_{,xx}^{(3)} \\
 & + \frac{16}{h^2} \left(-B_{12} (\mathbf{N}_{,x}^{(1)})^T \mathbf{N}^{(4)} + B_{22} (\mathbf{N}_{,xx}^{(2)})^T \mathbf{N}^{(4)} + \frac{4}{3h^2} B_{44} (\mathbf{N}_{,xx}^{(3)})^T \mathbf{N}^{(4)} \right) \\
 & \left. + \left(C_{11} - \frac{8}{h^2} C_{22} + \frac{16}{h^4} C_{44} \right) \left((\mathbf{N}_{,x}^{(2)})^T \mathbf{N}_{,x}^{(2)} + (\mathbf{N}_{,x}^{(2)})^T \mathbf{N}_{,x}^{(3)} + (\mathbf{N}_{,x}^{(3)})^T \mathbf{N}_{,x}^{(3)} \right) \right] dx
 \end{aligned} \tag{21}$$

In the above equation, $\mathbf{N}^{(i)}$ denotes the i^{th} row of the matrix of the interpolation matrix \mathbf{N} . The work done by the distributed load can be rewritten as

$$V = \sum^{nELE} \mathbf{d}^T \mathbf{f} \tag{22}$$

with \mathbf{f} is the consistent nodal load vector with the following form

$$\mathbf{f} = \int_0^\ell \left[\mathbf{N}^{(2)} + \mathbf{N}^{(3)} + \mathbf{N}^{(4)} \right]^T q(x) dx \tag{23}$$

The derived element stiffness matrix and nodal load vector are assembled into structural matrix and vector to form the equilibrium equation which can be written in the form [40]

$$\mathbf{K}\mathbf{D} = \mathbf{F} \tag{24}$$

where \mathbf{K} is the structural stiffness matrix; \mathbf{D} and \mathbf{F} are the structural nodal displacement and load vectors, respectively. Having the nodal displacements \mathbf{D} obtained from Eq. (24), the normal and shear stresses are then determined.

5. NUMERICAL RESULTS AND DISCUSSION

This section reports the bending behavior of the 2D-FGSW beam under various type of distributed load, namely uniform, linear, parabolic and sinusoidal as illustrated in Figure 2. To this end, a beam formed from Alunina and Aluminum with the geometric and material data given in Ref. [35] is employed herewith. Three types of boundary conditions, namely simply supported at (SS), clamped (CC) at both ends and clamped at the right end and free at the other (CF) are considered herewith.

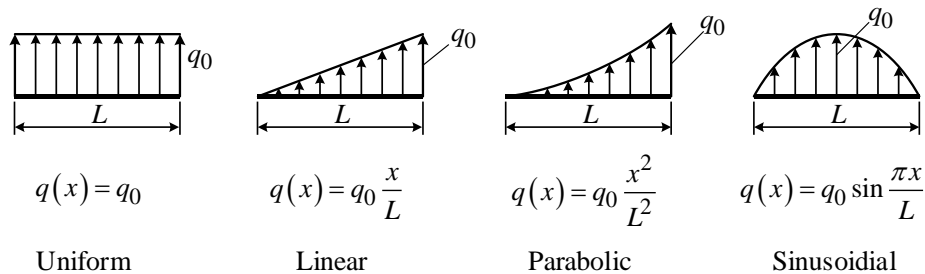


Figure 2. Type of distributed loads.

To facilitate the numerical discussion, the following dimensionless parameters are introduced for the deflection and stresses

$$w^* = \frac{100E_m b h^3}{q_0 L^4} w(x, 0), \quad \sigma_x^* = \frac{bh}{q_0 L} \sigma_x, \quad \sigma_z^* = \frac{bh}{q_0 L} \sigma_z, \quad \tau_{xz}^* = \frac{bh}{q_0 L} \tau_{xz} \quad (25)$$

where $w(x, 0)$, σ_x , σ_z and τ_{xz} are the mid-plane deflection, normal and shear stresses, respectively.

5.1. Formulation verification

Before computing the elastostatic response of the beam, the convergence and accuracy of the derived finite formulation and the developed computer code are firstly verified. The convergence of the formulation is shown in Table 1, where the maximum dimensionless deflections of the SS beam with $L/h = 20$ under the uniform load obtained are given for different number of the elements and various values of the material indexes and layer thickness ratio. In the tables and hereafter, the numbers in the brackets are employed to denote the skin-core-skin thickness ratio as used in [32], for example (2-2-1) = ($h_1:h_2:h_3$), with $h_i = z_i - z_{i-1}$ ($i = 1, 2, 3$). The convergence rate of the formulation, as seen from Table 1, depends on the material indexes and the layer thickness ratio as well. The convergence is a bit slower for the beam associated with the odd indexes and asymmetric layers, but it can be achieved by using twenty elements, regardless of the material indexes and the layer thickness ratio. In this regard, twenty elements are used to discrete the beam in all computations reported below.

Table 1. Convergence of the formulation in evaluating maximum dimensionless deflection (w^*) of SS beam with $L/h = 20$ under uniform distributed load.

$(p_x,$ $p_z)$	$nELE$	(1-1-1)	(1-2-1)	(1-8-1)	(2-2-1)
(0.5, 0.5)	10	6.2346	5.4019	3.8073	5.76 60
	12	6.2346	5.4019	3.8073	5.76 62
	14	6.2346	5.4019	3.8073	5.76 64
	16	6.2346	5.4019	3.8073	5.76 65
	18	6.2346	5.4019	3.8073	5.76 66
	20	6.2346	5.4019	3.8073	5.76 66
(2,2)	4	3.7283	3.5399	3.1634	3.63 41
	6	3.7285	3.5400	3.1634	3.63 44

	8	3.7285	3.5400	3.1634	3.63 45
	10	3.7285	3.5400	3.1634	3.63 45

The maximum dimensionless deflections of the SS and CC beams subjected to the uniform distributed load obtained in the present work are compared with the result of Ref. [37] in Tables 2 and 3. Very good agreement between the finite element solution of the present work with the result of Ref. [37] can be seen from the tables, regardless of the material indexes, the skin-core-skin and aspect ratios.

5.2. Deflections

Tables 4-6 list the dimensionless mid-span deflections of the SS beam under the linear, parabolic and sinusoidal loads for various values of the material indexes, the skin-core-skin thickness ratio and the aspect ratio, respectively. The effect of the material indexes, the skin-core-skin thickness ratio and the aspect ratio on the deflection of the beam under the nonuniform loading is similar to that of the beam under uniform load as reported in [37]. The mid-span deflection increases with an increase of the thickness index p_z and decreases with an increase of the length index p_x .

Table 2. Comparison of maximum dimensionless deflection of SS beams under uniform load.

p_x	p_z	Source	$L/h = 5$			$L/h = 20$		
			1-1-1	1-8-1	2-2-1	1-1-1	1-8-1	2-2-1
0.1	0.1	Ref. [37]	10.7054	4.7401	10.9470	10.3994	4.4818	9.1047
		Present	10.8634	4.8064	9.4128	10.4116	4.4848	9.1096
	0.5	Ref. [37]	7.5039	4.2112	9.5412	7.2199	3.9561	6.5597
		Present	7.6124	4.2698	6.8473	7.2273	3.9586	6.5680
	1	Ref. [37]	6.0343	3.9030	6.9428	5.7613	3.6501	5.3608
		Present	6.1185	3.9570	5.6327	5.7667	3.6525	5.3658
	2	Ref. [37]	4.8871	3.6275	4.6673	4.6274	3.3772	4.4070
		Present	4.9572	3.6775	4.7321	4.6313	3.3793	4.4101
0.5	0.1	Ref. [37]	8.4793	4.4862	5.7112	8.1706	4.4143	7.3680
		Present	8.6148	4.5492	7.6764	8.1964	4.2298	7.3839
	0.5	Ref. [37]	6.5069	4.0580	7.7882	6.2253	4.2331	5.7569
		Present	6.6011	4.1143	6.0408	6.2338	3.8040	5.7660
	1	Ref. [37]	5.4735	3.8004	6.1257	5.2055	3.8068	4.9004
		Present	5.5523	3.8534	5.1692	5.2114	3.5490	4.9064
	2	Ref. [37]	4.6040	3.5666	4.4251	4.3451	3.3169	4.1669
		Present	4.6689	3.6155	4.4873	4.3491	3.3190	4.1706
1	0.1	Ref. [37]	6.9827	4.2462	6.4602	6.6753	3.5515	6.1562
		Present	7.0975	4.3050	6.5600	6.7054	3.9922	6.1781
	0.5	Ref. [37]	5.7178	3.9088	5.3861	5.4388	3.9943	5.1050
		Present	5.8019	3.9608	5.4616	5.4499	3.6551	5.1153

	1	Ref. [37]	4.9904	3.6976	4.7624	4.7252	3.6570	4.4948
		Present	5.0598	3.7487	4.8272	4.7288	3.4477	4.5000
	2	Ref. [37]	4.3387	3.5031	4.1978	4.0816	3.2549	3.9396
		Present	4.3982	3.5514	4.2549	4.0843	3.2566	3.9434

The increase of the mid-span deflection by increasing p_z can be explained, as seen from Eq. (1), by the higher content of metal in the FGM skin layers, and this leads to the lower rigidities of the beam. Eq. (1) also shows a lower content of metal in the FGM skin layers when p_x is higher, and this leads to the decrease in the maximum deflection of the beam associated with a higher index p_x . Table 4-6 also show the effect of the loading type on the maximum deflection of the beam, and among the three types of the loading shown in the tables, the sinusoidal load gives the highest mid-span deflection while the parabolic results in the lowest one. The influence of the loading type on the maximum deflection of the 2D-FGSW beam can also be seen clearly from Figures 3-5, where the deformed configurations of (1-2-1) 2D-FGSW beam with ($p_x = 0.5$, $p_z = 1$) are illustrated for SS, CC and CF beams, respectively. Regardless of the boundary conditions, the beam deforms more significantly under the uniform load while it does the least under the parabolic load. Moreover, the deformed configurations of the SS and CC beams are unsymmetrical with respect to the centerline of the beam. Thus, it is necessary to note that the maximum deflections of the SS and CC beam are not always attained at the mid-span.

Table 3. Comparison of maximum dimensionless deflection of CC beams under uniform loads.

p_x	p_z	Source	$L/h = 5$			$L/h = 20$		
			1-1-1	1-8-1	2-2-1	1-1-1	1-8-1	2-2-1
0.1	0.1	Ref. [37]	2.4305	1.1824	2.2046	2.0753	0.9077	1.8245
		Present	2.4371	1.1837	2.1761	2.0791	0.9056	1.8231
	0.5	Ref. [37]	1.7642	1.0686	1.6311	1.4620	0.8030	1.3356
		Present	1.7678	1.0706	1.6338	1.4496	0.8010	1.3195
	1	Ref. [37]	1.4552	1.0026	1.3714	1.1650	0.7422	1.0883
		Present	1.4565	1.0043	1.3742	1.1601	0.7401	1.0808
	2	Ref. [37]	1.2108	0.9424	1.1653	0.9378	0.6891	0.8983
		Present	1.2135	0.9446	1.1673	0.9346	0.6857	0.8908
0.5	0.1	Ref. [37]	1.9858	1.1265	1.8104	1.6482	0.8572	1.4934
		Present	1.9899	1.1277	1.8232	1.6492	0.8547	1.4873
	0.5	Ref. [37]	1.5574	1.0352	1.4622	1.2333	0.7726	1.1470
		Present	1.5596	1.0364	1.4634	1.2530	0.7702	1.1599
	1	Ref. [37]	1.3351	0.9794	1.2733	1.0580	0.7224	1.0167
		Present	1.3373	0.9813	1.2748	1.0488	0.7195	0.9886
	2	Ref. [37]	1.1506	0.9288	1.1123	0.8825	0.6835	0.8826
		Present	1.1516	0.9307	1.1145	0.8777	0.6734	0.8424
1	0.1	Ref. [37]	1.7019	1.0774	1.5903	1.3804	0.8127	1.2779
		Present	1.7041	1.0786	1.5903	1.3777	0.8096	1.2680
	0.5	Ref. [37]	1.4053	1.0046	1.3330	1.1099	0.7451	1.0410
		Present	1.4074	1.0051	1.3364	1.1096	0.7417	1.0413

	1	Ref. [37]	1.2405	0.9571	1.1924	0.9476	0.7051	0.9078
		Present	1.2420	0.9598	1.1933	0.9597	0.7000	0.9131
	2	Ref. [37]	1.0965	0.9153	1.0674	0.8389	0.6555	0.7934
		Present	1.0977	0.9174	1.0679	0.8277	0.6614	0.7995

Table 4. The dimensionless mid-span deflection of SS beams under linear load.

P_x	P_z	$L/h = 5$				$L/h = 20$			
		1-1-1	1-2-1	1-8-1	2-2-1	1-1-1	1-2-1	1-8-1	2-2-1
0.1	0.1	5.4184	4.3008	2.4070	4.7622	5.1900	4.1058	2.2440	4.5439
	0.5	3.8048	3.1908	2.1391	3.4715	3.6099	3.0131	1.9814	3.2818
	1	3.0613	2.6651	1.9829	2.8582	2.8831	2.4971	1.8285	2.6832
0.5	0.1	4.2506	3.5917	2.2712	3.8504	4.0432	3.4098	2.1114	3.6497
	0.5	3.2756	2.8554	2.0569	3.0429	3.0929	2.6849	1.9013	2.8634
	1	2.7634	2.4705	1.9281	2.6114	2.5918	2.3065	1.7752	2.4417
1	0.1	3.4776	3.0698	2.1439	3.2228	3.2843	2.8964	1.9871	3.0342
	0.5	2.8648	2.5744	1.9766	2.7014	2.6902	2.4106	1.8230	2.5295
	1	2.5091	2.2946	1.8732	2.3961	2.3445	2.1356	1.7218	2.2332
2	0.1	2.7146	2.5083	1.9737	2.5817	2.5372	2.3449	1.8221	2.4072
	0.5	2.4008	2.2370	1.8645	2.3067	2.2361	2.0799	1.7137	2.1436
	1	2.1994	2.0690	1.7944	2.1298	2.0415	1.9157	1.6450	1.9731

Table 5. The dimensionless mid-span deflection of SS beams under parabolic load.

P_x	P_z	$L/h = 5$				$L/h = 20$			
		1-1-1	1-2-1	1-8-1	2-2-1	1-1-1	1-2-1	1-8-1	2-2-1
0.1	0.1	3.2164	2.5547	1.4314	2.8277	3.0818	2.4397	1.3350	2.6990
	0.5	2.2607	1.8965	1.2726	2.0630	2.1458	1.7917	1.1790	1.9510
	1	1.8196	1.5845	1.1799	1.6991	1.7145	1.4853	1.0881	1.5958
0.5	0.1	2.5040	2.1222	1.3483	2.2717	2.3809	2.0140	1.2541	2.1524
	0.5	1.9384	1.6922	1.2218	1.8021	1.8296	1.5913	1.1300	1.6954
	1	1.6382	1.4658	1.1459	1.5486	1.5368	1.3692	1.0555	1.4487
1	0.1	2.0386	1.8062	1.2711	1.8930	1.9261	1.7033	1.1787	1.7817
	0.5	1.6888	1.5217	1.1731	1.5946	1.5851	1.4242	1.0825	1.4924
	1	1.4840	1.3593	1.1124	1.4184	1.3860	1.2650	1.0231	1.3214
2	0.1	1.5874	1.4717	1.1688	1.5122	1.4849	1.3757	1.0788	1.4108
	0.5	1.4113	1.3189	1.1055	1.3581	1.3137	1.2255	1.0167	1.2613
	1	1.2976	1.2235	1.0648	1.2580	1.2037	1.1322	0.9768	1.1648

Table 6. The dimensionless mid-span deflection of SS beams under sinusoidal load.

P_x	P_z	$L/h = 5$				$L/h = 20$			
		1-1-1	1-2-1	1-8-1	2-2-1	1-1-1	1-2-1	1-8-1	2-2-1
0.1	0.1	8.5760	6.7981	3.7972	7.5330	8.2097	6.4857	3.5364	7.1831
	0.5	6.0111	5.0376	3.3738	5.4830	5.6989	4.7532	3.1216	5.1791
	1	4.8325	4.2054	3.1270	4.5112	4.5473	3.9366	2.8802	4.2312
0.5	0.1	6.7983	5.7226	3.5942	6.1471	6.4594	5.4264	3.3380	5.8197
	0.5	5.2127	4.5338	3.2511	4.8379	4.9149	4.2586	3.0019	4.5462
	1	4.3855	3.9139	3.0453	4.1411	4.1092	3.6510	2.8005	3.8687

1	0.1	5.5982	4.9186	3.4012	5.1757	5.2808	4.6354	3.1494	4.8666
	0.5	4.5797	4.1023	3.1298	4.3118	4.2946	3.8353	2.8836	4.0313
	1	3.9962	3.6466	2.9626	3.8129	3.7280	3.3893	2.7200	3.5478
2	0.1	4.3877	4.0352	3.1387	4.1622	4.0955	3.7678	2.8930	3.8752
	0.5	3.8532	3.5769	2.9576	3.6952	3.5835	3.3207	2.7156	3.4285
	1	3.5138	3.2964	2.8419	3.3979	3.2564	3.0467	2.6024	3.1425

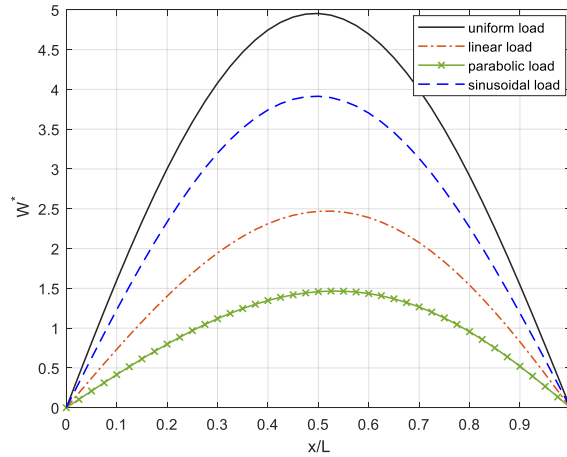


Figure 3. Deformed configurations of (1-2-1) SS beam with ($p_x = 0.5, p_z = 1$) under different types of distributed load ($L/h = 5$).

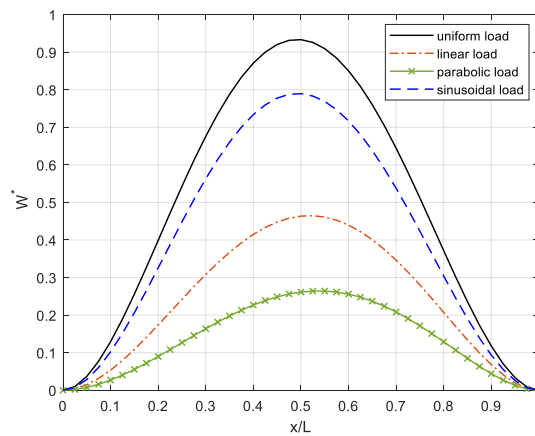


Figure 4. Deformed configurations of (1-2-1) CC beam with ($p_x = 0.5, p_z = 1$) under different types of distributed load ($L/h = 20$).

5.3. Normal stresses

Table 7-9 list the values of the dimensionless normal stress σ_x^* at the upper point of the mid-span section, $(x, z) = (L/2, h/2)$, for the SS beam under linear, parabolic and sinusoidal loads, respectively. Different from the deflection, at a given value of the skin-core-skin thickness ratio, the normal stress σ_x^* decreases with an increase of p_z but it increases by increasing p_x . The normal stress, as seen from the tables, is significantly influenced by the aspect ratio L/h , and the

normal stress σ_x^* is higher for the beam having a larger aspect ratio, regardless of the loading type. As in case of the deflection, the sinusoidal load results in significantly high normal stress comparing the linear and parabolic loads.

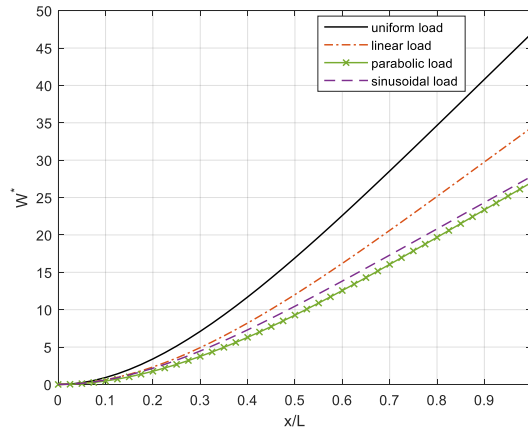


Figure 5. Deformed curves of (1-2-1) of CF beam with ($p_x = 0.5, p_z = 1$) under different types of distributed load ($L/h = 10$).

Table 7. The dimensionless normal stress $\sigma_x^* \left(\frac{L}{2}, \frac{h}{2} \right)$ of SS beams under linear loads.

p_x	p_z	$L/h = 5$				$L/h = 20$			
		1-1-1	1-2-1	1-8-1	2-2-1	1-1-1	1-2-1	1-8-1	2-2-1
0.1	0.1	1.4111	1.1159	0.6102	1.1095	5.6168	4.4366	2.4149	4.4054
	0.5	0.9810	0.8189	0.5387	0.8236	3.8967	3.2489	2.1305	3.2658
	1	0.7835	0.6787	0.4971	0.6855	3.1075	2.6891	1.9650	2.7156
0.5	0.1	1.5581	1.3163	0.8152	1.2870	6.1947	5.2288	3.2252	5.1072
	0.5	1.1946	1.0372	0.7333	1.0333	4.7414	4.1131	2.8997	4.0954
	1	1.0012	0.8907	0.6842	0.8940	3.9691	3.5277	2.7046	3.5401
1	0.1	1.6604	1.4718	1.0153	1.4307	6.5927	5.8408	4.0160	5.6720
	0.5	1.3698	1.2298	0.9306	1.2186	5.4324	4.8738	3.6793	4.8265
	1	1.1965	1.0906	0.8783	1.0899	4.7405	4.3179	3.4712	4.3140
2	0.1	1.7627	1.6424	1.2937	1.6003	6.9862	6.5086	5.1154	6.3352
	0.5	1.5724	1.4692	1.2178	1.4524	6.2280	5.8169	4.8135	5.7473
	1	1.4434	1.3579	1.1687	1.3524	5.7137	5.3728	4.6186	5.3498

The variation of the dimensionless normal stress σ_x^* on the thickness and longitudinal directions of (1-2-1) SS beam with $p_x = 0.5, p_z = 1$ is shown in Figure 6 for different types of loading and an aspect ratio $L/h = 20$. The corresponding figures for the CC beam and CF beam are depicted in Figures 7 and 8, respectively. The effect of the loading type on the stress distribution is clearly seen from the figures, where the amplitude of the normal stress is significantly altered when the beam is subjected to different types of the distributed load, regardless of the boundary conditions. The boundary conditions have also play an important role on the variation of the normal stress σ_x^* . As seen from Figure 7, the normal stress of the CC beam sharply changes in both the thickness and length direction, while the of this stress is

moderate for the SS and CF beams. For the normal stress σ_z^* , as illustrated in Figure 9 for the SS beam, its variation is much depend on the loading type. The unsymmetry of the normal stress σ_z^* with respect to the mid-line of the beam is clearly seen for the cases of linear and parabolic loads.

Table 8. The dimensionless normal stress $\sigma_x^*\left(\frac{L}{2}, \frac{h}{2}\right)$ of SS beams under parabolic loads.

P_x	P_z	$L/h = 5$				$L/h = 20$			
		1-1-1	1-2-1	1-8-1	2-2-1	1-1-1	1-2-1	1-8-1	2-2-1
0.1	0.1	0.8225	0.6503	0.3554	0.6470	3.2761	2.5877	1.4084	2.5708
	0.5	0.5716	0.4771	0.3137	0.4800	2.2728	1.8949	1.2426	1.9055
	1	0.4564	0.3953	0.2894	0.3994	1.8124	1.5684	1.1461	1.5843
0.5	0.1	0.9080	0.7670	0.4747	0.7503	3.6132	3.0498	1.8811	2.9803
	0.5	0.6960	0.6042	0.4270	0.6022	2.7655	2.3989	1.6912	2.3895
	1	0.5832	0.5188	0.3984	0.5208	2.3150	2.0575	1.5774	2.0653
1	0.1	0.9674	0.8574	0.5912	0.8338	3.8453	3.4068	2.3423	3.3096
	0.5	0.7980	0.7163	0.5419	0.7100	3.1685	2.8427	2.1459	2.8159
	1	0.6969	0.6352	0.5114	0.6349	2.7649	2.5184	2.0245	2.5167
2	0.1	1.0269	0.9567	0.7533	0.9324	4.0748	3.7962	2.9835	3.6961
	0.5	0.9159	0.8557	0.7091	0.8461	3.6325	3.3927	2.8074	3.3529
	1	0.8406	0.7908	0.6805	0.7877	3.3325	3.1336	2.6937	3.1208

Table 9. The dimensionless normal stress $\sigma_x^*\left(\frac{L}{2}, \frac{h}{2}\right)$ of SS beams under sinusoidal loads.

P_x	P_z	$L/h = 5$				$L/h = 20$			
		1-1-1	1-2-1	1-8-1	2-2-1	1-1-1	1-2-1	1-8-1	2-2-1
0.1	0.1	2.2906	1.8119	0.9920	1.7997	9.1074	7.1938	3.9160	7.1383
	0.5	1.5933	1.3303	0.8759	1.3373	6.3185	5.2681	3.4548	5.2929
	1	1.2729	1.1029	0.8083	1.1136	5.0389	4.3605	3.1865	4.4017
0.5	0.1	2.5301	2.1378	1.3251	2.0887	10.0442	8.4783	5.2300	8.2758
	0.5	1.9404	1.6852	1.1923	1.6782	7.6881	6.6694	4.7022	6.6375
	1	1.6268	1.4475	1.1126	1.4524	6.4360	5.7204	4.3858	5.7384
1	0.1	2.6968	2.3908	1.6505	2.3229	10.6895	9.4707	6.5123	9.1918
	0.5	2.2254	1.9984	1.5131	1.9794	8.8085	7.9030	5.9663	7.8230
	1	1.9443	1.7726	1.4280	1.7709	7.6867	7.0017	5.6289	6.9930
2	0.1	2.8639	2.6688	2.1032	2.5997	11.3277	10.5535	8.2950	10.2683
	0.5	2.5552	2.3878	1.9800	2.3600	10.0986	9.4322	7.8056	9.3165
	1	2.3460	2.2073	1.9004	2.1980	9.2649	8.7122	7.4896	8.6727

5.4. Shear stress

The effect of the loading type on the shear stress of the 2D-FGSW beam can be seen from Figure 10, where the variation of the dimensionless shear stress τ_{xz}^* along the beam length and the thickness directions is illustrated for the SS beam with $L/h = 20$ under different types of the distributed loads. As seen from the figure, the amplitude of the shear stress is changed considerably by the loading type, and the surfaces of the stress for the uniform and sinusoidal loads are similar, but they are significant different from that of the linear and parabolic loads.

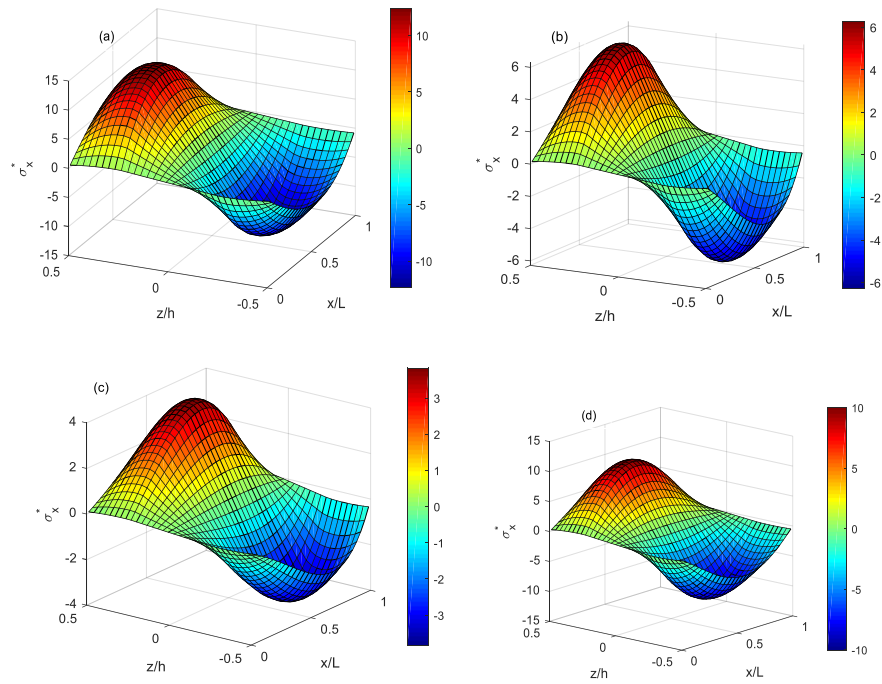


Figure 6. Variation of stress σ_x^ on the thickness and longitudinal directions of (1-2-1) SS beam with $L/h = 20$ under different loading types: (a) uniform, (b) linear, (c) parabolic, (d) sinusoidal.*

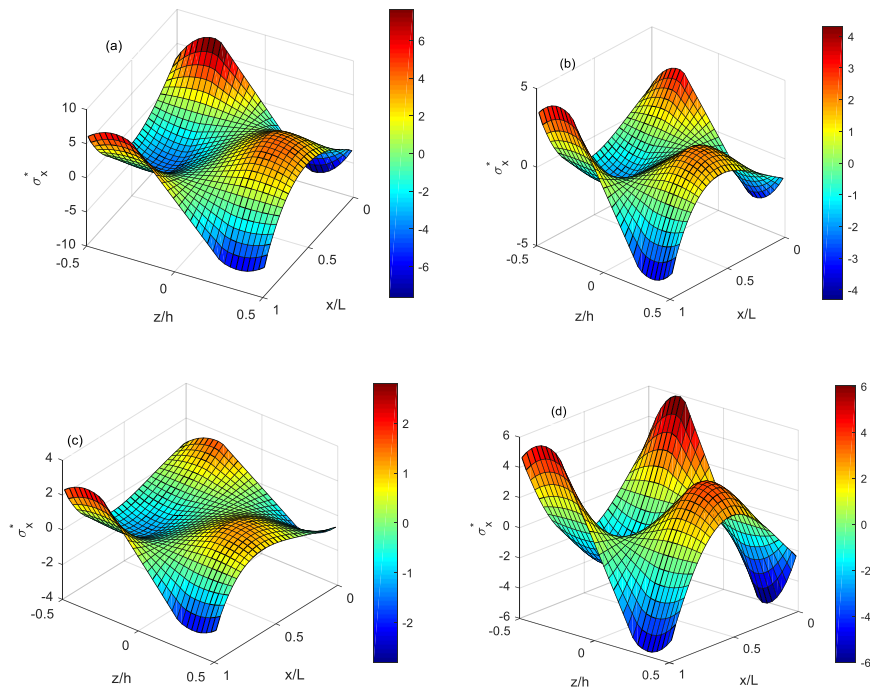


Figure 7. Variation of stress σ_x^ on the thickness and longitudinal directions of (1-2-1) CC beam with $L/h = 20$ under different loading types: (a) uniform, (b) linear, (c) parabolic, (d) sinusoidal.*

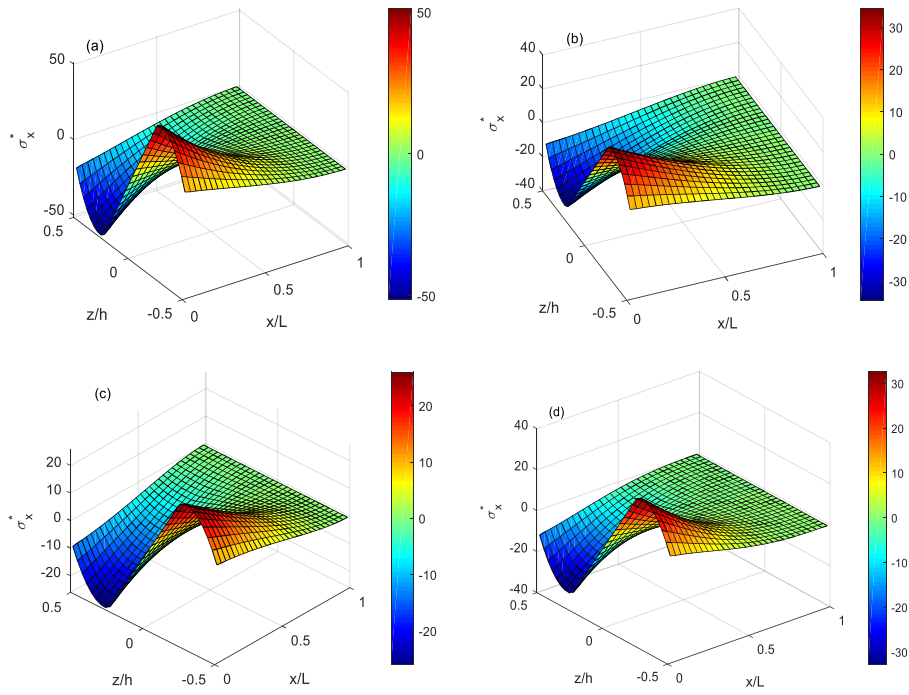


Figure 8. Variation of stress σ_x^* on the thickness and longitudinal directions of (1-2-1) CF beam with $L/h = 20$ under different loading types: (a) uniform, (b) linear, (c) parabolic, (d) sinusoidal.

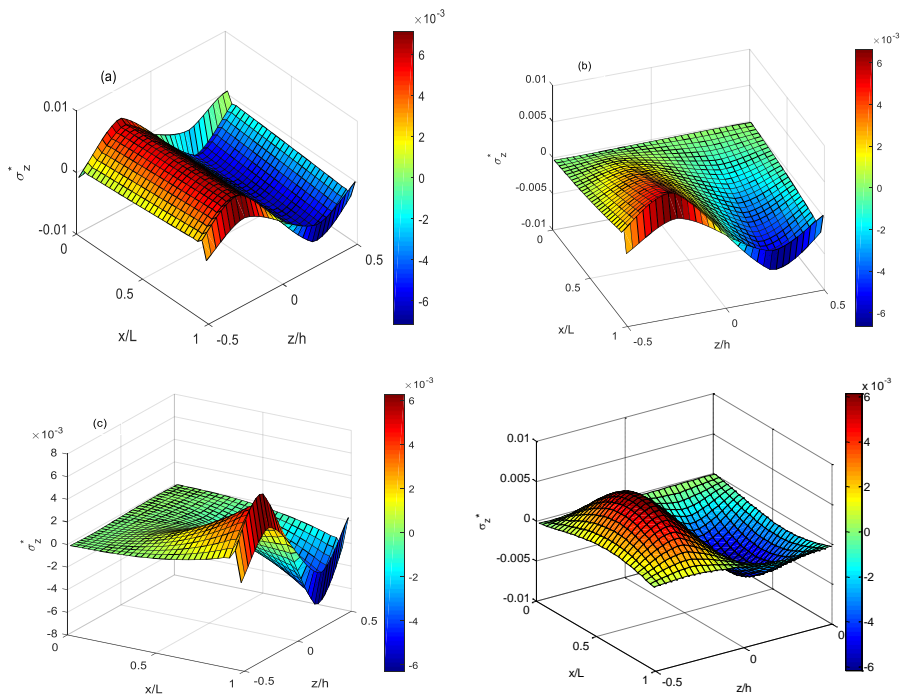


Figure 9. Variation of stress σ_z^* on the thickness and longitudinal directions of (1-2-1) SS beam with $L/h = 20$ under different loading: (a) uniform, (b) linear, (c) parabolic, (d) sinusoidal.

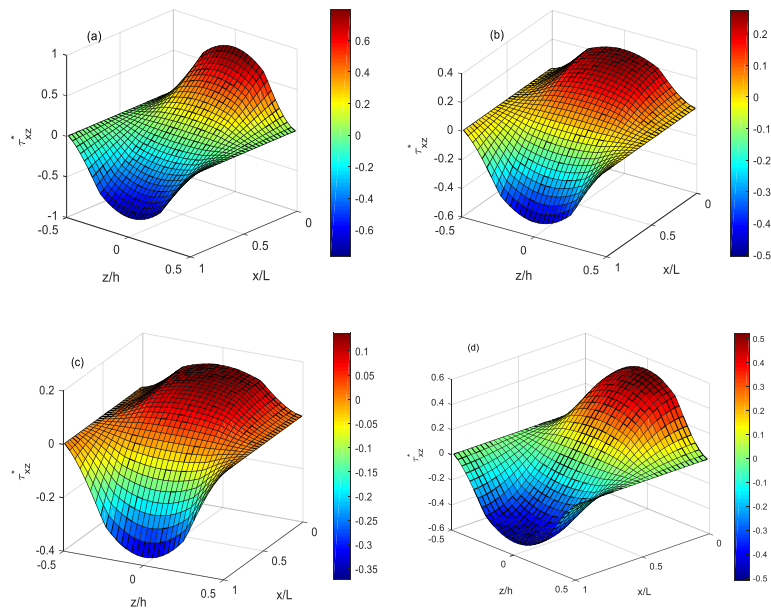


Figure 10. Variation of stress τ_{xz}^* on thickness and longitudinal directions of (1-2-1) SS beam with $L/h = 20$ under different loading type: (a) uniform, (b) linear, (c) parabolic, (d) sinusoidal.

6. CONCLUSIONS

The elastostatic behavior of a 2D-FGSW beam under various types of nonuniform distributed load has been investigated by a finite element procedure. The beam is considered to be formed from a homogeneous hardcore and 2D-FGM skin layers. Based on the quasi-3D shear deformation beam theory, a finite element model has been derived and employed to compute the elastostatic response of the beam. The accurate of the derived formulation in evaluating the bending characteristics of the beams has been confirmed though an comparison study. The obtained numerical results reveal that in addition to the thickness material index, the gradation of the longitudinal exponent also pay an important role in the elastostatic behavior of the beams. The elastostatic response, in terms of maximum deflection and stresses, of the beams under the nonuniform loading is not significant comparing to that of the beam due to uniform loading, regardless of the boundary conditions. A parametric study has been carried out to illustrate the influence of the material distribution, the skin-core-skin thickness and aspect ratios on the response of the beams. The effect of the loading type on the deflections and the distribution of the normal and shear stresses has also been examined and highlighted.

REFERENCES

1. Sina S. A., Navazi H. M., and Haddadpour H. - An analytical method for free vibration analysis of functionally graded beams. *Materials and Design* **30** (2009) 741–747.
2. Li X. F. - A unified approach for analyzing static and dynamic behaviours of functionally graded Timoshenko and Euler- Bernoulli beams, *Journal of Sound and Vibration* **318** (2008) 1210-1229.

3. Alshorbagy A. E., Eltaher M. A., and Mahmoud F. F. - Free vibration characteristics of a functionally graded beam by finite element method, *Applied Mathematical Modelling* **35** (2011) 412-425.
4. Shahba A., Attarnejad R., and Hajilar S. - Free vibration and stability of axially functionally graded tapered Euler-Bernoulli beams, *Shock and Vibration* **18** (2011) 683-696.
5. Wattanasakulpong N., and Ungbhakorn V. - Linear and nonlinear vibration analysis of elastically restrained ends FGM beams with porosities, *Aerospace Science and Technology* **32** (2014) 111-120.
6. Şimşek M., and Kocatürk T. - Free and forced vibration of a functionally graded beam subjected to a concentrated moving harmonic load, *Composite Structures* **90** (2009) 465-473.
7. Şimşek M. - Vibration analysis of a functionally graded beam under a moving mass by using different beam theories, *Composite Structure* **92** (2010) 904-917.
8. Chen D., Yang J., and Kitipornchai S. - Free and forced vibrations of shear deformable functionally graded porous beams, *International Journal of Mechanical Sciences* **108-109** (2016) 14-22.
9. Gan B. S., Trinh T. H., Le T. H., and Nguyen D. K. - Dynamic response of non-uniform Timoshenko beams made of axially FGM subjected to multiple moving point loads, *Structural Engineering and Mechanics* **53** (2015) 981-995.
10. Nguyen D. K., and Bui V. T. - Dynamic analysis of functionally graded Timoshenko beams in thermal environment using a higher-order hierarchical beam element, *Mathematical Problems in Engineering* (2017) <https://doi.org/10.1155/2017/7025750>
11. Benatta M. A., Mechab I., Tounsi A., and Adda Bedia E. A. - Static analysis of functionally graded short beams including warping and shear deformation effects, *Computational Material Science* **44** (2008) 765-773.
12. Kadoli R., Akhtar K., and Ganesan N. - Static analysis of functionally graded beams using higher order shear deformation theory, *Applied Mathematical Modelling* **32** (2008) 2509-2525.
13. Thai H. T., and Vo T. P. - Bending and free vibration of functionally graded beams using various higher-order shear deformation beam theories, *International Journal of Mechanical Science* **62** (2012) 57-66.
14. Vo T. P., Thai H. T., Nguyen T. K., and Inam F. - Static and vibration analysis of functionally graded beams using refined shear deformation theory, *Meccanica* **49** (2014) 155-168.
15. Nguyen D. K., and Gan B. S. - Large deflections of tapered functionally graded beams subjected to end forces, *Applied Mathematical Modelling* **38** (2014) 3054-3066.
16. Huang Y., and Li X.-F. - Buckling analysis of nonuniform and axially graded columns with varying flexural rigidity, *Journal of Engineering Mechanics* **137** (2011) 73-81.
17. Shahba A., Attarnejad R., Marvi M. T., and Hajilar S. - Free vibration and stability analysis of axially functionally graded tapered Timoshenko beams with classical and non-classical boundary conditions, *Composites Part B Engineering* **42** (2011) 801-808.

18. Shahba A., and Rajasekaran S. - Free vibration and stability of tapered Euler–Bernoulli beams made of axially functionally graded materials, *Applied Mathematical Modelling* **36** (2012) 3094–3111.
19. Nemat-Alla M., and Noda N. - Edge crack problem in a semi-infinite FGM plate with a bi-directional coefficient of thermal expansion under two-dimensional thermal loading, *Acta Mechanica* **144** (2000) 211–229.
20. Lü C. F., Chen W. Q., Xu R. Q., and Lim C.W. - Semi-analytical elasticity solutions for bi-directional functionally graded beams, *International Journal of Solids Structures* **45** (2008) 258-275.
21. Şimşek M.- Bi-directional functionally graded materials (BDFGMs) for free and forced vibration of Timoshenko beams with various boundary conditions, *Composite Structures* **133** (2015) 968-997.
22. Hao D., and Wei C. - Dynamic characteristics analysis of bi-directional functionally graded Timoshenko beams, *Composite Structures* **141** (2016) 253-263.
23. Lezgy-Nazargah M. - Fully coupled thermo-mechanical analysis of bi-directional FGM beams using NURBS isogeometric finite element approach, *Aerospace Science and Technology* **45** (2015) 154-164.
24. Wang Z., Wang X., Xu G., Cheng S., and Zeng T. - Free vibration of two-directional functionally graded beams, *Composite Structures* **135** (2016) 191-198.
25. Nguyen D. K., Nguyen Q. H., Tran T. T., and Bui V. T. - Vibration of bi-dimensional functionally graded Timoshenko beams excited by a moving load, *Acta Mechanica* **228** (2017) 141-155.
26. Tran T. T., and Nguyen D. K. - Free vibration of two-directional FGM beam using a higher-order Timoshenko beam element, *Vietnam Journal of Science and Technology* **56** (2018) 380-396.
27. Nguyen D. K., and Tran T. T. – Free vibration of tapered BFGM beams using an efficient shear deformable finite element model, *Steel and Composite Structures* **29** (2018) 363-377.
28. Pydah A., and Sabale A. - Static analysis of bi-directional functionally graded curved beams, *Composite Structures* **160** (2017) 867-876.
29. Li J., Guan Y., Wang G., Zhao G., Lin J., Naceur H., and Coutellier D. - Meshless modeling of bending behavior of bi-directional functionally graded beam structures, *Composites Part B* **155** (2018) 104-111.
30. Tang Y, Lv X., and Yang T. - Bi-directional functionally graded beams: asymmetric modes and nonlinear free vibration, *Composites Part B* **156** (2019) 319-331.
31. Bui T. Q., Khosravifard A., Zhang Ch., Hematiyan M. R., and Golub M. V. - Dynamic analysis of sandwich beams with functionally graded core using a truly meshfree radial point interpolation method, *Engineering Structures* **47** (2013) 90-104.
32. Vo T. P., Thai H. T., Nguyen T. K., Maheri A., and Lee J. - Finite element model for vibration and buckling of functionally graded sandwich beams based on a refined shear deformation theory, *Engineering Structures* **64** (2014) 12-22.
33. Vo T. P., Thai H. T., Nguyen T. K., Inam F., and Lee J. - A quasi-3D theory for vibration and buckling of functionally graded sandwich beams, *Composite Structures* **119** (2015) 1-12.

34. Vo P. T., Thai H. T., Nguyen T. K., Inam F., and Lee J. - Static behaviour of functionally graded sandwich beams using a quasi-3D theory, *Composites Part B: Engineering* **68** (2015) 59-74.
35. Nguyen D. K., and Tran T. T. - A corotational formulation for large displacement analysis of functionally graded sandwich beam and frame structures, *Mathematical Problems in Engineering*, <http://dx.doi.org/10.1155/2016/5698351>
36. Su Z., Jin G., Wang Y., and Ye X. - A general Fourier formulation for vibration analysis of functionally graded sandwich beams with arbitrary boundary condition and resting on elastic foundations, *Acta Mechanica* **227** (2016) 1493–1514.
37. Karamanli A. - Bending behaviour of two directional functionally graded sandwich beams by using a quasi-3d shear deformation theory, *Composite Structures* **174** (2017) 70–86.
38. Bickford W. B. - A consistent higher order beam theory, *Development of Theoretical and Applied Mechanics, SECTAM* **11** (1982) 137-50.
39. Reddy J. N. - A simple higher-order theory for laminated composite plates, *Journal of Applied Mechanics* **51** (1984) 745-752.
40. Cook R D., Malkus D. S., and Plesha M. E. - *Concepts and Applications of Finite Element Analysis*, 3rd edition, John Willey & Sons, New York, 1989.